

How to Manipulate Through-Space Conjugation and Clusteroluminescence of Simple AIEgens with Isolated Phenyl Rings

Jianguo Zhang, Lianrui Hu, Kaihua Zhang, Junkai Liu, Xingguang Li, Haoran Wang, Zhaoyu Wang, Herman H. Y. Sung, Ian D. Williams, Zebing Zeng, Jacky W. Y. Lam, Haoke Zhang,* and Ben Zhong Tang*

Cite This: *J. Am. Chem. Soc.* 2021, 143, 9565–9574

Read Online

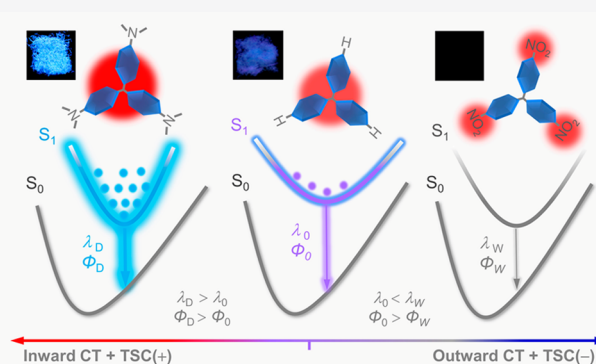
ACCESS |

Metrics & More

Article Recommendations

Supporting Information

ABSTRACT: Apart from the traditional through-bond conjugation (TBC), through-space conjugation (TSC) is gradually proved as another important interaction in photophysical processes, especially for the recent observation of clusteroluminescence from non-conjugated molecules. However, unlike TBC in conjugated chromophores, it is still challenging to manipulate TSC and clusteroluminescence. Herein, simple and nonconjugated triphenylmethane (TPM) and its derivatives with electron-donating and electron-withdrawing groups were synthesized, and their photophysical properties were systematically studied. TPM was characterized with visible clusteroluminescence due to the intramolecular TSC. Experimental and theoretical results showed that the introduction of electron-donating groups into TPM could redshift the wavelength and increase the efficiency of clusteroluminescence simultaneously, due to the increased electronic density and stabilization of TSC. However, TPM derivatives with electron-withdrawing groups showed inefficient or even quenched clusteroluminescence caused by the vigorous excited-state intramolecular motion and intermolecular photoinduced electron transfer process. This work provides a reliable strategy to manipulate TSC and clusteroluminescence.



INTRODUCTION

The use of light is the starting point for human civilization. Beginning from the fifth century B.C., when philosophers of ancient Greece raised the question about the essence of light, humanity started to investigate and utilize natural sources of light.¹ In modern society, because of the deeper cognition on science and technology, people began to design artificial emitters, especially luminogens, which can emit efficiently upon photoexcitation.^{2–5} Therefore, what are the laws behind the luminescent behaviors and how to design and manipulate artificial luminophores at different levels of hierarchical structures are important issues, as evidenced by the Nobel Prize for the discovery of green fluorescent protein and the invention of efficient blue-light-emitting diodes in 2008 and 2014, respectively.

Compared with inorganic materials, organic fluorophores show better flexibility, biocompatibility, processability, structural diversity, etc. Thus, they show great promise in practical applications. Researchers have established many photophysical theories based on molecular science, which focus on the fluorescent mechanisms of organic fluorophores. For example, efficient fluorophores are closely correlated with large π conjugation through covalent bonds (e.g., double bond, triple

bond, or aromatic ring),^{6,7} and introduction of donor (D) and acceptor (A) groups into the molecular skeleton often leads to redder but weaker emission,^{8,9} especially for molecules showing twisted intramolecular charge transfer effects.^{10,11} In most cases, these molecular theories are capable of revealing the photophysical mechanisms of organic luminescent materials. Based on these studies at the molecular level, a paradigm of material research is gradually formed that molecular structures and properties always determine the performance of macroscopic materials. However, due to the continuous development of photophysical research, some abnormal phenomena were reported sporadically that aggregates possessed entirely different properties from single-molecule species. One example is the aggregation-caused quenching (ACQ) effect, where most fluorophores are highly emissive in solution but become nonemissive in the aggregate

Received: April 13, 2021

Published: June 11, 2021



state.¹² In contrast, some invisible phenomena of molecules in the isolated state could be observed in the aggregate state,^{13–15} such as the aggregation-induced emission (AIE) effect. Luminoogens with the AIE effect (AIEgens) are nonemissive in dilute solution but luminesce strongly in the aggregate state. The flourishing development of ACQ- and AIE-related studies brings a paradigm shift from molecular science to aggregate science.^{16–18}

Recent research in aggregate science has reported that many nonconjugated structures, such as polystyrene,¹⁹ peptide,²⁰ maleimide,²¹ and some polymers bearing poorly conjugated groups,^{22,23} are nonemissive in solution but can emit visible light in the solid state. This unconventional photophysical process is termed clusterization-triggered emission, and the corresponding emission is known as clusteroluminescence.^{24–27} The previous studies suggested that strong intermolecular interactions among the closely packed molecules generated new emissive species and stabilized excited excitons to produce clusteroluminescence.^{28–30} Apart from intermolecular interaction, intramolecular through-space conjugation (TSC) was also proved to play an important role in clusteroluminescence. For example, our recent study revealed that nonconjugated 1,1,2,2-tetraphenylethane with weak intermolecular interactions fluoresced efficiently in the aggregate state, and the intramolecular TSC among the four phenyl rings contributed greatly to the clusteroluminescence.³¹ Based on the above results, two common questions have emerged: (i) is TSC a general mechanism for clusteroluminescence, and (ii) is it possible to manipulate TSC in clusteroluminoogens?

In this work, nonconjugated triphenylmethane (TPM) and its derivatives with different electron-donating and -withdrawing groups, namely, 4,4',4''-trimethoxytriphenylmethane (TPM-MO), 4,4',4''-tris(*N,N*-dimethylaminophenyl)methane (TPM-DMA), 4,4',4''-tricyanotriphenylmethane (TPM-CN), and 4,4',4''-trinitrotriphenylmethane (TPM-NO₂), were synthesized and satisfactorily characterized (Figures S1–S11 in the Supporting Information). All the molecules showed visible light in the solid state with different colors and efficiency. Experimental and theoretical results proved that TSC was also applicable to these clusteroluminoogens. The electron-donating groups in TPM-MO and TPM-DMA could red-shift the wavelength and increase the efficiency of clusteroluminescence simultaneously by enhancing the TSC. However, the electron-withdrawing groups in TPM-CN and TPM-NO₂ decentralized the electrons of phenyl rings and destabilized the intramolecular TSC, resulting in low emission efficiency. On the other hand, restriction of intramolecular motions (RIM),³² which served as the mechanism of the AIE phenomenon, helped to stabilize the preferential conformation for TSC in the aggregate state. The synergistic effect between TSC and RIM generated efficient clusteroluminescence of TPM and its derivatives. Thus, this study not only verified the general mechanism of TSC in clusteroluminoogens but also provided a reliable strategy to manipulate clusteroluminescence at the molecular level.

RESULTS AND DISCUSSION

2.1. Photophysical Properties. TPM is a simple molecule with three isolated phenyl rings and was first prepared to study its photophysical properties. The absorption spectra of TPM in both THF solution and the solid state exhibited an absorption maximum (λ_{ab}) corresponding to benzene rings at 264 nm,

confirming the nonconjugated nature of the molecule (Figure 1a). In pure THF solution, TPM showed one emission peak at

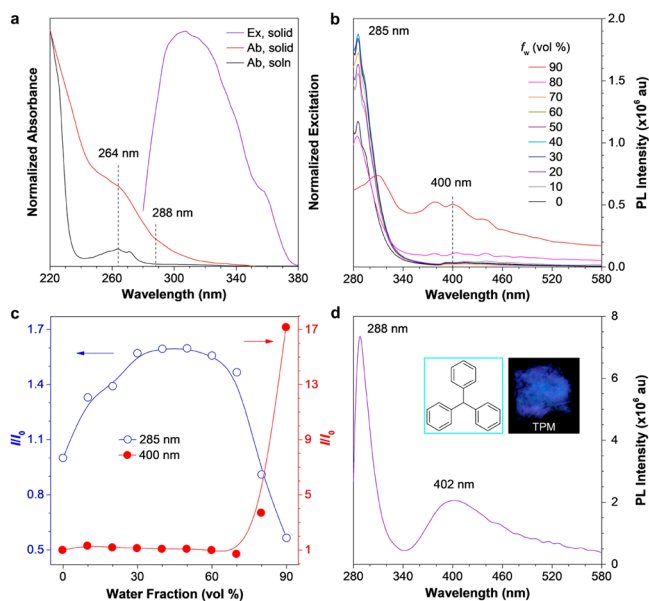


Figure 1. (a) Absorption (Ab) spectra of TPM in THF solution (soln) and the solid state. Concentration (c) = 10^{-4} M. Inset: Excitation (Ex) spectrum in the solid state taken at $\lambda_{em} = 402$ nm. (b) Photoluminescence (PL) spectra of TPM in THF/water mixtures with different water fractions (f_w). $c = 10^{-4}$ M, $\lambda_{ex} = 270$ nm. (c) Plots of relative PL intensity (I/I_0) versus f_w at different emission wavelengths. $c = 10^{-4}$ M, $\lambda_{ex} = 270$ nm, I_0 = intensity at $f_w = 0\%$. (d) PL spectra of TPM in the solid state taken at $\lambda_{ex} = 270$ nm. Inset: Structure and fluorescent photo of TPM taken under illumination of a 365 nm UV lamp.

285 nm, which was attributed to the intrinsic through-bond conjugation (TBC) of benzene. Addition of poor solvent such as water into the THF solution induced the formation of TPM aggregates (Figure 1b). During the aggregation process, the emission intensity at 285 nm first increased and then decreased, and the turning point was located at a water fraction (f_w) of 50% in volume. It was noteworthy that a new broad emission peak appeared at 350–380 nm at $f_w = 80–90\%$, and its intensity at 400 nm was 17 times higher than that in pure THF solution (Figure 1c). This long-wavelength emission demonstrated the AIE phenomenon and might be attributed to the formation of stable through-space interaction in the aggregate state that gave rise to clusteroluminescence.³¹ At an f_w of less than 50%, the enhancement of TBC emission was due to the increased polarity of the solvent mixture.³³ However, aggregates only formed at high $f_w \geq 80\%$ (Figures S12–S15), and the internal polarity of aggregates was less affected by the surrounding environment of the mixture. Meanwhile, a portion of excited energy of TBC was transferred to TSC species via the Förster resonance energy transfer (FRET) process, where TBC and TSC species acted as donor and acceptor, respectively, which finally decreased the emission from TBC but increased the emission from TSC. The solid-state emission spectrum of TPM showed two maxima (λ_{em}) at 288 and 402 nm under 270 nm excitation (Figure 1d), which were assigned to the intrinsic emission from TBC of phenyl rings and clusteroluminescence with TSC, respectively. The excitation spectrum of TPM in the solid state exhibited a long-wavelength peak at 310 nm, suggesting the formation of new

emissive species by TSC. Thus, only one peak with a fluorescence quantum yield (Φ_{TSC}) of 2.7% appeared at 403 nm with 310 nm excitation (Figure S16).

The above results proved the existence of clusteroluminescence in TPM but with a low Φ . To adjust the through-space interaction among the three phenyl rings, electron-donating methoxy groups were introduced to increase the electron density of each phenyl ring. The obtained TPM-MO showed an λ_{ab} at 278 nm in THF solution (Figure 2a), which was

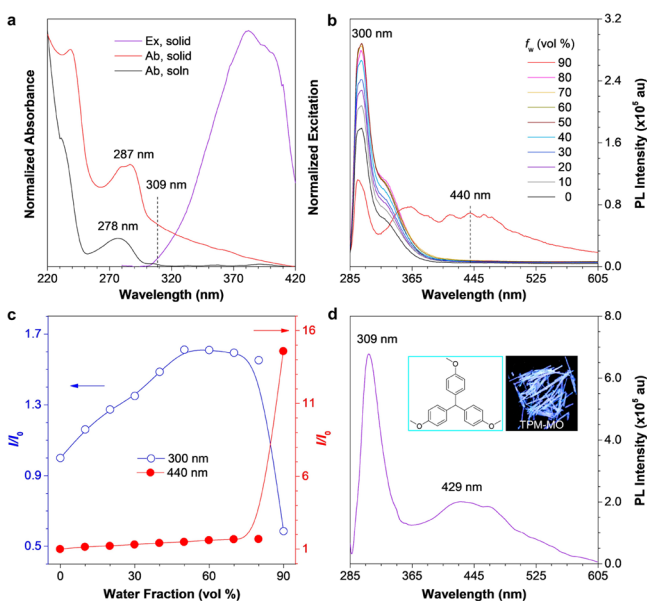


Figure 2. (a) Absorption (Ab) spectra of TPM-MO in THF solution (soln) and the solid state. Concentration (c) = 10^{-4} M. Inset: Excitation (Ex) spectrum in the solid state taken at λ_{em} = 429 nm. (b) Photoluminescence (PL) spectra of TPM-MO in THF/water mixtures with different water fractions (f_w). $c = 10^{-4}$ M, λ_{ex} = 280 nm. (c) Plots of relative PL intensity (I/I_0) versus f_w at different emission wavelengths. $c = 10^{-4}$ M, λ_{ex} = 280 nm, I_0 = intensity at $f_w = 0\%$. (d) PL spectra of TPM-MO in the solid state taken at λ_{ex} = 280 nm. Inset: Structure and fluorescent photo of TPM-MO taken under illumination of a 365 nm UV lamp.

similar to that of anisole (Figure S17). The λ_{ab} shifted bathochromically to 287 nm in the solid state. TPM-MO emitted short-wavelength emission at 300 nm in a THF/water mixture, and its intensity also first increased but later decreased by increasing f_w (Figure 2b and c). At the same time, a new broad peak at ~ 440 nm was observed at $f_w = 90\%$, whose intensity was 15 times higher than that in pure THF solution. Also, the emission spectrum was well extended to 600 nm. The solid-state emission spectrum of TPM-MO exhibited two emission peaks at 309 and 429 nm at λ_{ex} = 280 nm, which originated from TBC and TSC, respectively (Figure 2d). The excitation spectrum of TPM-MO also showed a broad peak at around 370 nm in the solid state. Upon excitation at 370 nm, the clusteroluminescence of TPM-MO was red-shifted to 439 nm and the Φ_{TSC} was enhanced to 6.3% in comparison to TPM with λ_{em} = 403 nm and Φ_{TSC} = 2.7%, respectively (Figure S16).

A strong electron-donating group, *N,N*-dimethylamino (DMA), was also utilized to construct TPM-DMA. Its λ_{ab} was located at 306 and 312 nm in pure THF solution and the solid state (Figure 3a), respectively, due to the better conjugation and donor (D)–acceptor (A) effect of DMA

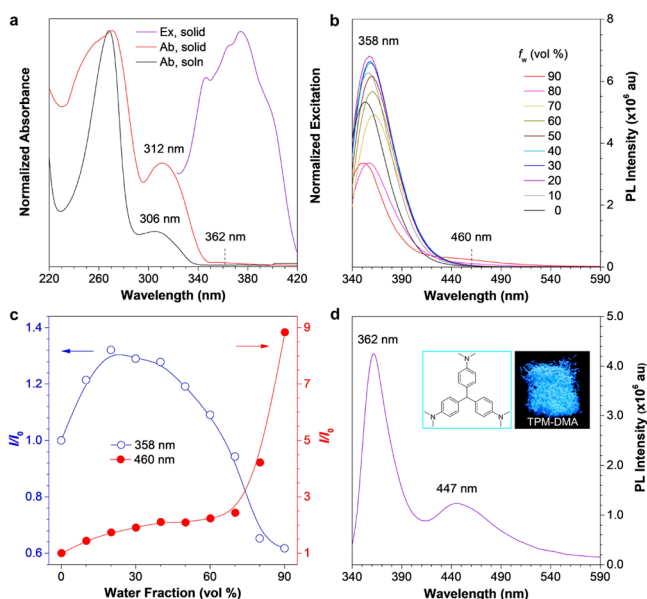


Figure 3. (a) Absorption (Ab) spectra of TPM-DMA in THF solution (soln) and the solid state. Concentration (c) = 10^{-4} M. Inset: Excitation (Ex) spectrum in the solid state taken at λ_{em} = 447 nm. (b) Photoluminescence (PL) spectra of TPM-DMA in THF/water mixtures with different water fractions (f_w). $c = 10^{-4}$ M, λ_{ex} = 320 nm. (c) Plots of relative PL intensity (I/I_0) versus f_w at different emission wavelengths. $c = 10^{-4}$ M, λ_{ex} = 320 nm, I_0 = intensity at $f_w = 0\%$. (d) PL spectra of TPM-DMA in the solid state taken at λ_{ex} = 320 nm. Inset: Structure and fluorescent photo of TPM-DMA taken under illumination of a 365 nm UV lamp.

and the phenyl ring. Figure 3b showed that only one emission peak was detected at 358 nm at low f_w , which was associated with the TBC of *N,N*-dimethylaniline (Figure S17). Similarly, TBC emission became weaker at an f_w of more than 50% (Figure 3c). A long-wavelength emission at 460 nm was observed at $f_w \geq 80\%$, and its intensity at $f_w = 90\%$ was 9-fold higher than that in pure THF solution. The intensity of this new band was somewhat lower than that of TPM-MO, which might be due to the vigorous motion of the DMA group and loose packing of aggregates in TPM-DMA. In the solid state, TPM-DMA exhibited bright sky-blue clusteroluminescence at λ_{em} = 447 nm and another invisible TBC emission at 362 nm with λ_{ex} = 320 nm (Figure 3d). When excited at the excitation maximum of 380 nm (Figure 3a), only the long-wavelength emission stemmed from TSC was observed at 453 nm (Figure S16). The corresponding Φ_{TSC} was 6.9%, which was slightly higher than that of TPM-MO (6.3%).

Considering that electron-donating moieties could bathochromically shift and enhance the Φ of clusteroluminescence, the effect of electron-withdrawing groups on TSC was further explored. Thus, cyano and nitro groups were selected as substituents to synthesize TPM-CN and TPM-NO₂, respectively. The λ_{ab} of TPM-CN in THF solution and the solid state were redder than TPM and both located at 282 nm (Figure 4a), corresponding to the TBC emission of benzonitrile (Figure S17). As shown in Figure 4b, only the emission of TBC (λ_{em} = 294 nm) was observed at low f_w and another long-wavelength peak located at 457 nm was noticed at $f_w = 90\%$ (Figure 4c). In the solid state, two emission peaks appeared at 300 and 460 nm with 270 nm excitation (Figure 4d). The inset in Figure 4a showed that the λ_{ex} was much longer than the λ_{ab} in the solid state. Therefore, upon excitation at 380 nm, only

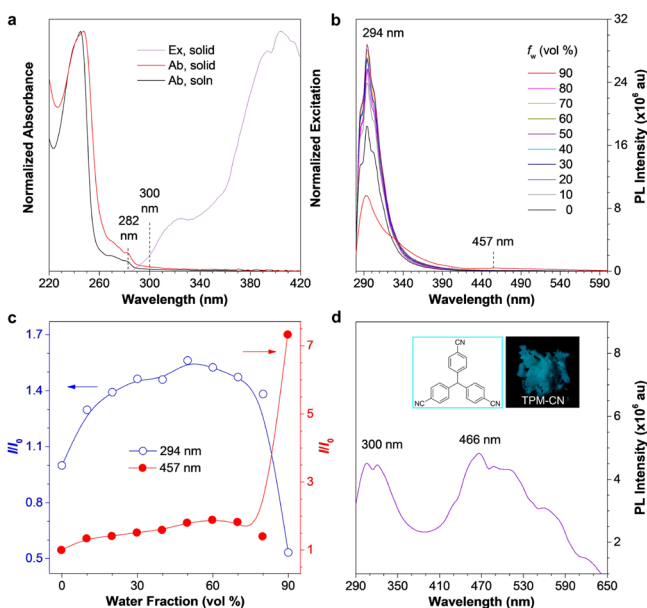


Figure 4. (a) Absorption (Ab) spectra of TPM-CN in THF solution (soln) and the solid state. Concentration (c) = 10^{-4} M. Inset: Excitation (Ex) spectrum in the solid state taken at $\lambda_{em} = 466$ nm. (b) Photoluminescence (PL) spectra of TPM-CN in THF/water mixtures with different water fractions (f_w). $c = 10^{-4}$ M, $\lambda_{ex} = 270$ nm. (c) Plots of relative PL intensity (I/I_0) versus f_w at different emission wavelengths. $c = 10^{-4}$ M, $\lambda_{ex} = 270$ nm, I_0 = intensity at $f_w = 0\%$. (d) PL spectra of TPM-CN in the solid state taken at $\lambda_{ex} = 270$ nm. Inset: Structure and fluorescent photo of TPM-CN taken under illumination of a 365 nm UV lamp.

one peak at 482 nm was detected, which was even redder than that of TPM-DMA ($\lambda_{em} = 453$ nm). The Φ_{TSC} of such TSC emission was low and was measured to be 2.2% at $\lambda_{ex} = 380$ nm, which was lower than that of TPM, TPM-MO, and TPM-DMA. For TPM-NO₂, its absorption maximum was redder than TPM, but its emission was quenched in both solution and the solid state at room temperature and could not be identified (Figure S19).

To exclude the interference from radical species that was reported to be responsible for some extrinsic emissions,^{34–36} electron spin resonance spectra of the present molecules were measured, but none of them showed obvious signals in the presence or absence of UV illumination (Figure S20). This result suggested the inherent emission of these stable structures. The photophysical properties of all molecules are summarized in Table 1 and Figure S21. It was noteworthy that the emission lifetime caused by TSC (τ_{TSC}) was longer than that due to TBC (τ_{TBC}), demonstrating the relatively stable excitons formed by through-space interaction (Figure S22). And the lifetime of TSC was more sensitive for molecular conformation and substituent groups than that of TBC. For example, the τ_{TSC} of TPM-DMA was measured to be 9.7 ns, which was three times longer than τ_{TBC} (3.3 ns). Besides, when the substituents were changed from electron-donating to electron-withdrawing groups, the τ_{TSC} became shorter and the Φ_{TSC} decreased from 6.9% in TPM-DMA to 0.4% in TPM-NO₂.

2.2. Through-Space Conjugation. To confirm TSC and investigate the electronic effect on clusteroluminescence, single-molecule calculations on present compounds were carried out. The density functional theory method at the

Table 1. Photophysical Properties of TPM and Its Derivatives (TPM-R)^a

TPM-R	λ_{ab} (nm)	$\lambda_{ex,solid}$ (nm)	TBC emission		TSC emission		Φ_{TSC} (%)
			λ_{TBC} (nm)	τ_{TBC} (ns)	λ_{TSC} (nm)	τ_{TSC} (ns)	
TPM-DMA	306	375	362	3.3	447	9.7	6.9
TPM-MO	278	382	309	2.6	429	3.6	6.3
TPM	264	307	288	<1.0	402	3.6	2.7
TPM-CN	282	404	305	<1.0	466	2.7	2.2
TPM-NO ₂	276						0.4

^aAbbreviation: λ_{ab} = absorption maximum in THF solution, $\lambda_{ex,solid}$ = excitation maximum in the solid state measured at emission maximum of 447 nm (TPM-DMA), 429 nm (TPM-MO), 402 nm (TPM), and 466 nm (TPM-CN). TBC = through-bond conjugation, λ_{TBC} = emission maximum through TBC in the solid state, τ_{TBC} = emission lifetime through TBC in the solid state, TSC = through-space conjugation, λ_{TSC} = emission maximum through TSC in the solid state, τ_{TSC} = emission lifetime through TSC in the solid state, Φ_{TSC} = absolute luminescence quantum yield at an excitation wavelength of 380 nm (TPM-DMA), 370 nm (TPM-MO), 310 nm (TPM), or 380 nm (TPM-CN).

B3LYP-D3/6-31G(d,p) level was utilized to calculate the ground- and excited-state geometries. The reference plane was constructed to illustrate the structural information, which was set as atoms of 1–2–3 in Table S1. At the ground state (S_0), all the optimized structures displayed a highly C₃-symmetrical and propeller-like conformation, as evidenced by the dihedral angles between the reference plane and each phenyl ring, which were around 55°. Frontier molecular orbitals at S_0 were shown in Figure S23, including electron cloud distribution and energy levels of the highest occupied molecular orbital (HOMO) and the lowest unoccupied molecular orbital (LUMO). Electrons at the HOMO were distributed on the phenyl rings and substituent groups.

However, the geometries and electronic effect became different at the excited state (S_1) (Table S1). The energy gap between the HOMO and LUMO of TPM derivatives was narrower than that of TPM (Figure 5), which was consistent with their redder λ_{ab} and λ_{em} through TBC. Besides, the values were smaller than the corresponding substituted phenyl rings such as benzene, *N,N*-dimethylaniline, anisole, benzonitrile, and nitrobenzene, suggesting the existence of intramolecular through-space interaction (Tables S2 and S3). As observed from the LUMO of TPM, a clear electronic overlapping among the three isolated phenyl rings was observed, which verified the effect of intramolecular TSC in TPM. For TPM-MO and TPM-DMA with electron-donating groups, apart from electronic overlapping, a noticeable D–A transition from the donor to phenyl ring was observed. Together with their symmetrical structures and the shortened atomic distances of 1–2, 2–3, and 3–1 at S_1 (Table S1), the dihedral angles between the reference plane and each phenyl ring decreased from 55° to around 46°. This indicated the closer distance between every two phenyl rings and more concentrated π electrons at the center of the molecular skeleton in comparison with S_0 . In TPM-CN, two phenyl rings displayed a nearly face-to-face conformation, while the other one was perpendicular to them. Such a parallel arrangement was beneficial for efficient TSC, even though it was a binary rather than a ternary TSC, as proved in our previous report.³¹ The parallel binary TSC caused a red-shift in clusteroluminescence from 402 to 466 nm (Figure 4d). For nitro-substituted TPM-NO₂, a dark (n, π^*)

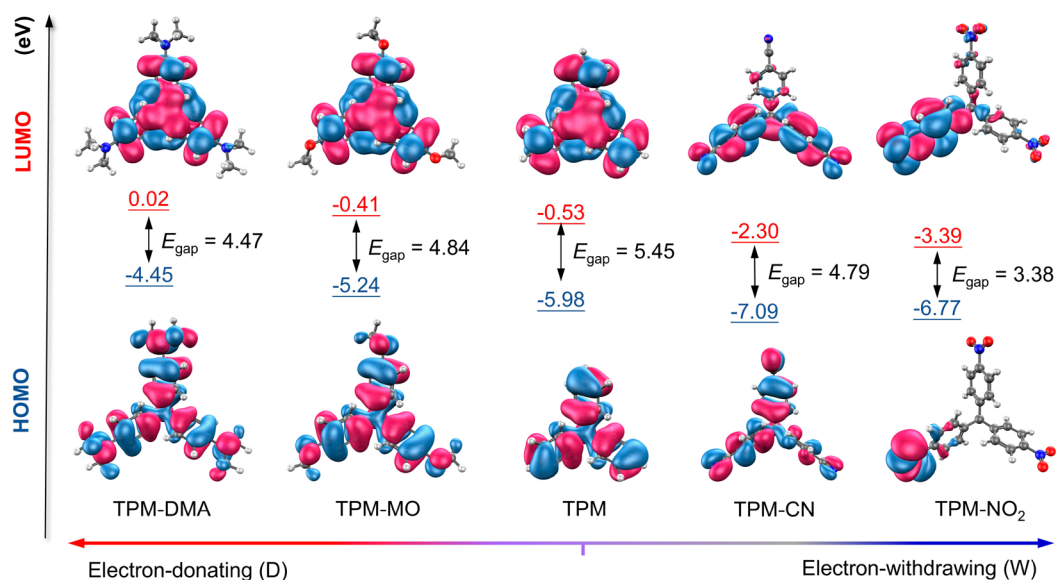


Figure 5. Frontier molecular orbitals of optimized excited-state geometries of TPM derivatives calculated by the TD-DFT method at the B3LYP-D3/6-31G(d,p) level, Gaussian 16 program.

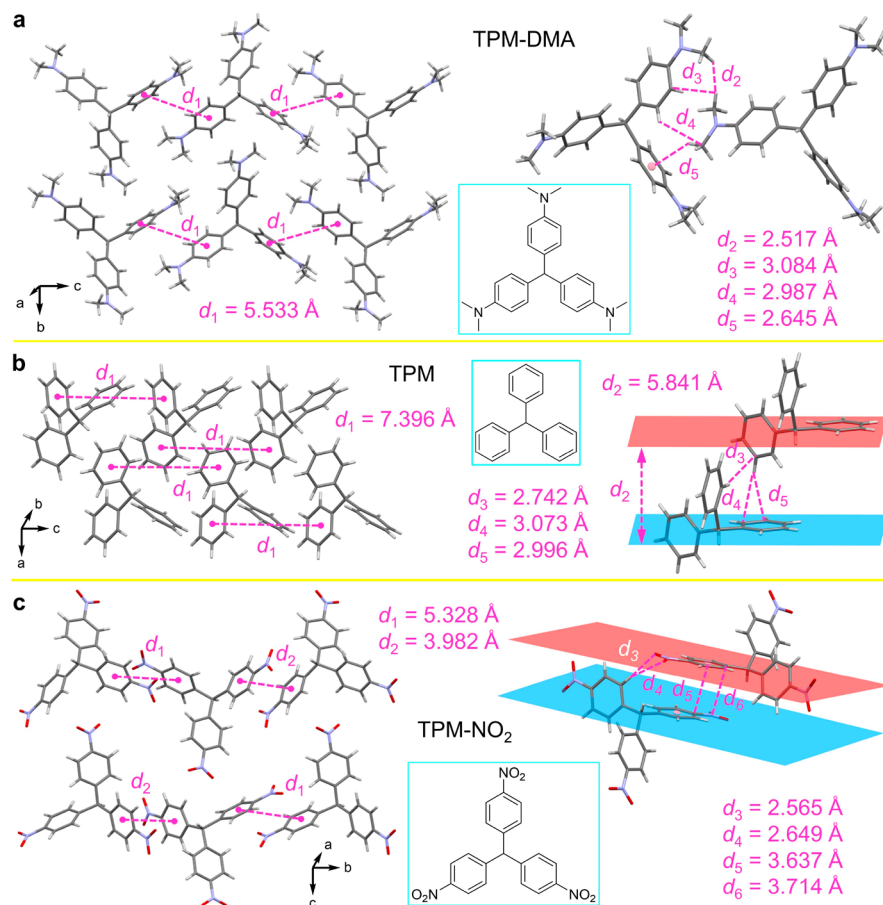


Figure 6. Crystal packing diagrams of (a) TPM-DMA, (b) TPM, and (c) TPM-NO₂.

transition showing no intramolecular TSC became dominant, deciphering its nonfluorescent behavior in the solution and aggregate state.³⁷

2.3. Crystal Structures. Single-molecule calculations had proved the important role of intramolecular TSC in clusteroluminescence of TPM derivatives, but how about the

intermolecular interaction? To explore the effect of intermolecular interaction on clusteroluminescence, crystal structures of all compounds were obtained and analyzed (Table S4). Figure 6 shows the crystal packing structures of TPM-DMA, TPM, and TPM-NO₂. In TPM-DMA, no parallel plane was observed and the centroid–centroid distance between two

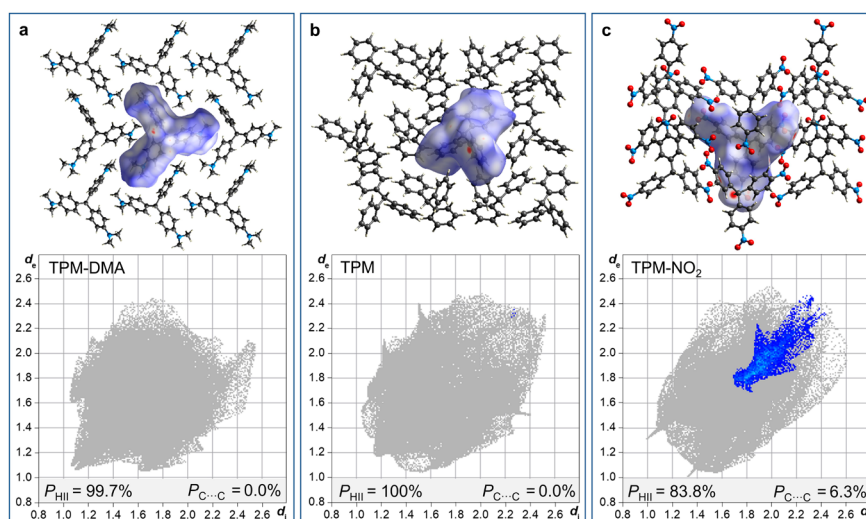


Figure 7. (Upper panel) Hirshfeld surfaces (mapped over d_{norm}) and (lower panel) decomposed fingerprint plots of (a) TPM-DMA, (b) TPM, and (c) TPM-NO₂. The full fingerprints appear as gray shadows underneath decomposed plots, and the intermolecular C...C interaction is shown as a blue shadow. P_{HII} = proportion of hydrogen-involved intermolecular interaction to total intermolecular interaction; $P_{\text{C}\cdots\text{C}}$ = proportion of intermolecular C...C interaction to total intermolecular interaction.

adjacent phenyl rings was 5.533 Å (Figure 6a). Instead, some weak intermolecular interactions such as C...H, C–H... π , and H...H were dominant. A quantitative analysis on intermolecular interactions based on the Hirshfeld surface was utilized.³⁸ As shown in Figure 7, the full fingerprints appeared as gray shadows and the selected interaction was shown with blue. Thus, in TPM-DMA, the hydrogen-involved intermolecular interaction (P_{HII}) accounted for 99.7% of all intermolecular interactions. No intermolecular C...C interaction was detected, suggesting the absence of strong intermolecular π – π stacking, which may quench emission (Figures 7a and S24). The same situation was observed in TPM-MO, which showed almost no intermolecular TSC (Figures S25 and S26). In TPM, although the two intermolecular phenyl rings were parallel to each other, the distance between the two planes was as far as 5.841 Å (Figure 6b) and the P_{HII} of TPM was up to 100% without intermolecular C...C interaction (Figures 7b and S27). Therefore, the above results suggested that the clusteroluminescence of TPM and its donor-based derivatives was a kind of intramolecular rather than intermolecular behavior, whereas these weak intermolecular interactions could restrict intramolecular motions and stabilize excitons with intramolecular TSC.^{32,39}

For electron-withdrawing TPM-CN and TPM-NO₂, the closest intermolecular C...C distances determined from the crystal packing structures were 3.442 and 3.637 Å, respectively, which suggested strong intermolecular π – π stacking (Figures 6c and S28). Meanwhile, intermolecular D–A interactions also existed, as proved by the presence of short intermolecular C...N distances. From the quantitative perspective, the proportion of intermolecular C...C interaction to total interactions ($P_{\text{C}\cdots\text{C}}$) in TPM-CN and TPM-NO₂ was 8.4% and 6.3%, respectively (Figures 7c, S29, and S30), which further confirmed the existence of intermolecular π – π stacking. Therefore, the redder clusteroluminescence of electron-withdrawing TPM derivatives than TPM resulted from both intramolecular and intermolecular through-space interactions. Meanwhile, the close packing of TPM-CN and TPM-NO₂ also resulted in the detrimental intermolecular photoinduced electron transfer from phenyl rings to cyano and nitro groups, which enhanced

the nonradiative decay and decreased the efficiency of clusteroluminescence.

2.4. Clusteroluminescence. Traditional clusteroluminogens based on macromolecular systems show ambiguous spatial conformations and interactions, which makes it difficult to clarify the photophysical process of clusteroluminescence. In contrast, the identified single-molecule and packing structures in the current system enable deep studies on the working mechanisms of clusterization-triggered emission. Reorganization energy (λ) is a quantitative indicator of intrinsic geometry change upon photoexcitation, which also reflects the contribution of intramolecular motion to nonradiative decay.^{40,41} Figure 8a exhibited a λ of TPM-DMA at different wavenumbers in the isolated phase as an example. The total λ was 2142 cm⁻¹, and 66.17% of it was contributed by the twisting motion of the dihedral angle located mainly in the low-frequency region (<500 cm⁻¹). The low-frequency vibration modes also tended to mix upon excitation to activate multiple nonradiative decay pathways. Hence, the potential energy surface (PES) of TPM-DMA in dilute solution was proposed and is displayed in Figure 8b. Upon photoexcitation to S₁, some excitons decayed via the radiative channel to produce TBC emission. At the same time, transient species with intramolecular TSC also formed but immediately evolved to the dark state near the conical intersection due to the vigorous low-frequency motions.⁴² As a result, only the TBC emission was detected. Based on the crystal packing structure of TPM-DMA, its aggregate environment was also simulated using the ONIOM model with a combined quantum mechanics and molecular mechanics (QM/MM) approach (Figure S31). The central molecule acted as the high layer with QM at the B3LYP-D3/6-31G(d,p) level, while the surrounding molecules acted as the low layer using the universal force field (UFF). The total λ in the aggregate state largely decreased to 1246 cm⁻¹, and the contribution of the dihedral angle also declined to 40.38% (Figure 8c), suggesting the restriction of intramolecular motion, especially twisting motion in the excited state. By combining experimental and theoretical results, Figure 8d illustrates the PES for TPM-DMA in the crystalline state. Similar to that in the solution state, some

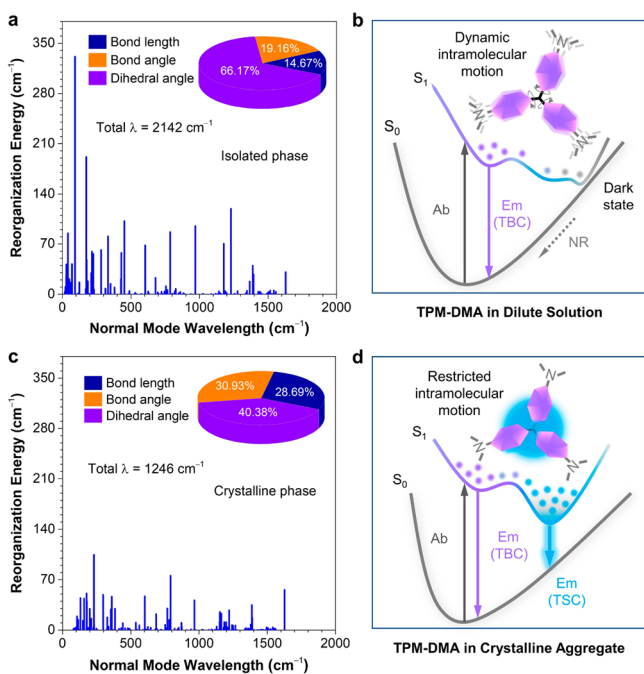


Figure 8. Plots of reorganization energy vs normal mode wavenumber of TPM-DMA in (a) isolated and (c) crystalline phases calculated by TD-DFT, B3LYP-D3/6-31G(d,p), and the Gaussian 16 program. Inset: Proportions of bond length, bond angle, and dihedral angle contributed to total reorganization energy. Potential energy surfaces of TPM-DMA in (c) solution and (d) aggregate states. Ab = absorption, Em = emission, and NR = nonradiative decay.

excited excitons were released from the channel of TBC emission. However, according to Kasha's rule, more excitons went to the low-lying state of TSC, which was further stabilized by restricted intramolecular motion. Thus, the nonradiative

decay channel was blocked and clusteroluminescence was realized with a comparatively high quantum yield.

Reorganization energy of other compounds in the isolated and crystalline phases was also calculated (Figures S32–S35). For TPM-MO and TPM, both total λ and the contribution of the dihedral angle became smaller in the crystalline phase than those in the isolated phase. Besides, the increased Φ_{TSC} from TPM (2.7%), then TPM-MO (6.3%), and to TPM-DMA (6.9%) was consistent with the enlarged $\Delta\lambda$ (the decrease of λ from the isolated to crystalline phase: 33 cm^{-1} for TPM, 514 cm^{-1} for TPM-MO, and 896 cm^{-1} for TPM-DMA), verifying that the restriction of intramolecular motion in the crystalline state had stabilized the TSC and boosted the emission efficiency of clusteroluminescence. However, the total λ of TPM-CN slightly increased from isolated (2857 cm^{-1}) to crystalline phase (3143 cm^{-1}), but the contribution of the dihedral angle reduced from 57.34% to 26.95% (Figure S34), which resulted in the decreased emission efficiency but redder clusteroluminescence among all molecules. So, within this molecule, intramolecular motion performs like a double-edged sword that produces the low-lying TSC state but cannot stabilize the excited-state through-space interaction. TPM-NO₂ is one of the extreme cases: its total λ was large and measured to be 7316 and 7370 cm^{-1} in the isolated and crystalline phases, which quenched the emission in both phases (Figure S35).

To investigate how electron-donating or -withdrawing groups affect TSC and clusteroluminescence, the excited-state electronic static potential based on electronic density was mapped. As shown in Figure 9a, the red parts represent high electronic density, while those in blue correspond to low density. Apparently, electron-donating groups provided more electrons to the central part of the molecular skeleton, as the red color was observed on the three phenyl rings of TPM-DMA and TPM-MO. TPM, as the basic compound, showed

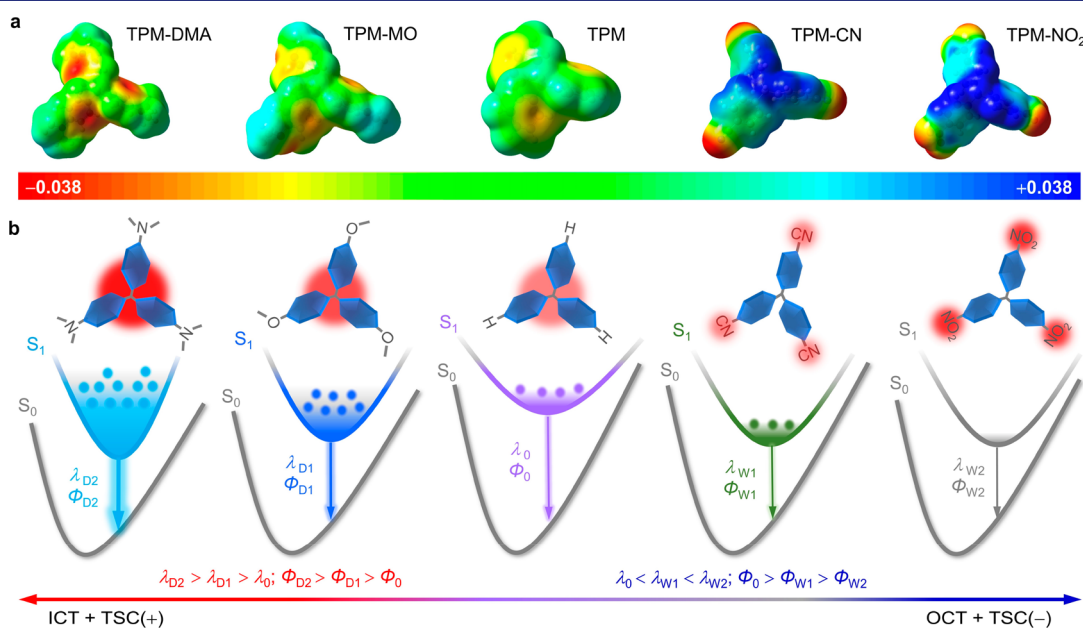


Figure 9. (a) Electronic static potential (ESP) mapped on the isosurface of electronic density, based on optimized excited-state geometries of TPM-R. A negative electrostatic potential (red) represents a high electronic density, whereas a positive one (blue) corresponds to low electronic density. The values of the potential are given in au. (b) First line: effects of charge transfer (CT) and TSC; second line: the proposed potential energy surfaces for the clusteroluminescence of TPM-R; ICT = inward charge transfer, OCT = outward charge transfer, + = stabilization/increment, – = destabilization/decrement.

lower electronic density at the central phenyl rings than its electron-donating derivatives. In contrast, TPM-CN and TPM-NO₂, with strong electron-withdrawing groups, exhibited low electronic density at the central phenyl rings, and the electrons were pulled to the exterior cyano and nitro groups. Accordingly, a complete picture of clusteroluminescence of these different systems was summarized from the perspective of intramolecular TSC (Figure 9b). In the excited state, electron-rich TPM derivatives pushed electrons from donors to the central phenyl rings, to trigger an inward charge transfer (ICT) process and stabilize the intramolecular TSC. Therefore, from TPM, then TPM-MO, and finally to TPM-DMA, the wavelength and efficiency of clusteroluminescence became longer and higher. In contrast, TPM derivatives with electron-withdrawing groups attracted electrons from the central phenyl rings to the exterior acceptors, to produce an outward charge transfer (OCT) and destabilize the TSC. Finally, TPM-CN and TPM-NO₂ showed inefficient clusteroluminescence, although the energy levels of their TSC states were lower than TPM and even their electron-rich cousins.

CONCLUSION

In this work, nonconjugated triphenylmethane and its derivatives with electron-donating (TPM-DMA and TPM-MO) and electron-withdrawing (TPM-CN and TPM-NO₂) groups were synthesized, and their photophysical properties were systematically investigated. Except TPM-NO₂, all the molecules exhibited dual emission in the aggregate state: a short-wavelength peak from TBC and a long-wavelength clusteroluminescence stemmed from TSC. Meanwhile, introduction of the electron-donating groups had been found to red-shift the wavelength and increase the efficiency of the clusteroluminescence at the same time. Crystal packing and theoretical calculation suggested that the addition of donors not only increased the electronic density for TSC but also stabilized the formed excitons by restricting the intramolecular motion. However, the introduction of acceptors decreased the emission efficiency, but still caused a bathochromic shift in clusteroluminescence. Different from TPM and the electron-donating counterparts, TPM-CN and TPM-NO₂ exhibited both intra- and intermolecular TSC to result in the reddest clusteroluminescence of TPM-CN. But the vigorous excited-state intramolecular motion and unfavorable intermolecular PET process destabilized the excited excitons to eventually quench the light emission. This work not only proves the general mechanism of through-space conjugation for clusteroluminescence in nonconjugated luminogens but also provides a reliable strategy to manipulate its emission efficiency and color simultaneously. It is anticipated that the development of TSC theories will establish a significant linkage between molecular and aggregate photophysics.

ASSOCIATED CONTENT

Supporting Information

The Supporting Information is available free of charge at <https://pubs.acs.org/doi/10.1021/jacs.1c03882>.

Materials and methods, synthetic procedures, characterization, crystallographic data (TPM-DMA, TPM-MO, TPM-CN, and TPM-NO₂), and computational details, including Figures S1–S35 and Tables S1–S14 (PDF)

Accession Codes

CCDC 2035370–2035372 and 2064012 contain the supplementary crystallographic data for this paper. These data can be obtained free of charge via www.ccdc.cam.ac.uk/data_request/cif, or by emailing data_request@ccdc.cam.ac.uk, or by contacting The Cambridge Crystallographic Data Centre, 12 Union Road, Cambridge CB2 1EZ, UK; fax: +44 1223 336033.

AUTHOR INFORMATION

Corresponding Authors

Ben Zhong Tang – Department of Chemistry, Hong Kong Branch of Chinese National Engineering Research Center for Tissue Restoration and Reconstruction and Institute for Advanced Study, The Hong Kong University of Science and Technology, Kowloon, Hong Kong 999077, China; Shenzhen Institute of Aggregate Science and Technology, School of Science and Engineering, The Chinese University of Hong Kong, Shenzhen 518172, China; AIE Institute, Guangzhou 510530, China; orcid.org/0000-0002-0293-964X; Email: tangbenz@cuhk.edu.cn

Haoke Zhang – MOE Key Laboratory of Macromolecular Synthesis and Functionalization, Department of Polymer Science and Engineering, Zhejiang University, Hangzhou 310027, China; Guangdong Provincial Key Laboratory of Luminescence from Molecular Aggregates, South China University of Technology, Guangzhou 510640, China; orcid.org/0000-0001-7309-2506; Email: zhanghaoke@zju.edu.cn

Authors

Jianyu Zhang – Department of Chemistry, Hong Kong Branch of Chinese National Engineering Research Center for Tissue Restoration and Reconstruction and Institute for Advanced Study, The Hong Kong University of Science and Technology, Kowloon, Hong Kong 999077, China; orcid.org/0000-0002-5213-7063

Lianrui Hu – Department of Chemistry, Hong Kong Branch of Chinese National Engineering Research Center for Tissue Restoration and Reconstruction and Institute for Advanced Study, The Hong Kong University of Science and Technology, Kowloon, Hong Kong 999077, China

Kaihua Zhang – State Key Laboratory of Chemo/Biosensing and Chemometrics, College of Chemistry and Chemical Engineering, Hunan University, Changsha 410082, China

Junkai Liu – Department of Chemistry, Hong Kong Branch of Chinese National Engineering Research Center for Tissue Restoration and Reconstruction and Institute for Advanced Study, The Hong Kong University of Science and Technology, Kowloon, Hong Kong 999077, China

Xingguang Li – Department of Chemistry, Hong Kong Branch of Chinese National Engineering Research Center for Tissue Restoration and Reconstruction and Institute for Advanced Study, The Hong Kong University of Science and Technology, Kowloon, Hong Kong 999077, China

Haoran Wang – Department of Chemistry, Hong Kong Branch of Chinese National Engineering Research Center for Tissue Restoration and Reconstruction and Institute for Advanced Study, The Hong Kong University of Science and Technology, Kowloon, Hong Kong 999077, China

Zhaoyu Wang – Department of Chemistry, Hong Kong Branch of Chinese National Engineering Research Center for Tissue Restoration and Reconstruction and Institute for Advanced Study, The Hong Kong University of Science and

Technology, Kowloon, Hong Kong 999077, China;

orcid.org/0000-0002-8453-643X

Herman H. Y. Sung – Department of Chemistry, Hong Kong Branch of Chinese National Engineering Research Center for Tissue Restoration and Reconstruction and Institute for Advanced Study, The Hong Kong University of Science and Technology, Kowloon, Hong Kong 999077, China

Ian D. Williams – Department of Chemistry, Hong Kong Branch of Chinese National Engineering Research Center for Tissue Restoration and Reconstruction and Institute for Advanced Study, The Hong Kong University of Science and Technology, Kowloon, Hong Kong 999077, China

Zebing Zeng – State Key Laboratory of Chemo/Biosensing and Chemometrics, College of Chemistry and Chemical Engineering, Hunan University, Changsha 410082, China;

orcid.org/0000-0002-6246-3911

Jacky W. Y. Lam – Department of Chemistry, Hong Kong Branch of Chinese National Engineering Research Center for Tissue Restoration and Reconstruction and Institute for Advanced Study, The Hong Kong University of Science and Technology, Kowloon, Hong Kong 999077, China

Complete contact information is available at:

<https://pubs.acs.org/10.1021/jacs.1c03882>

Notes

The authors declare no competing financial interest.

ACKNOWLEDGMENTS

This work was partially supported by the National Natural Science Foundation of China Grants (51773076, 21871060, 81271476, and 31870991), the Innovation and Technology Commission (ITC-CNERC14SC01), the Research Grants Council of Hong Kong (16305518, 16307020, C6014-20W, C6009-17G, and N-HKUST609/19), and the Material Science Foundation of Guangdong Province (2019B121205012 and 2019B030301003). H.Z. is thankful for the support from the Fundamental Research Funds for the Central Universities (2021QNA4032) and the Open Fund of Guangdong Provincial Key Laboratory of Luminescence from Molecular Aggregates and South China University of Technology.

REFERENCES

- (1) Al-Amri, M. D.; El-Gomati, M. M.; Zubairy, M. S. *Optics in Our Time*; Springer Nature, 2016; pp 4–24.
- (2) Wei, Q.; Fei, N.; Islam, A.; Lei, T.; Hong, L.; Peng, R.; Fan, X.; Chen, L.; Gao, P.; Ge, Z. Small-Molecule Emitters with High Quantum Efficiency: Mechanisms, Structures, and Applications in OLED Devices. *Adv. Opt. Mater.* **2018**, *6*, 1800512.
- (3) Xu, W.; Wang, D.; Tang, B. Z. NIR-II AIEgens: A Win-Win Integration Towards Bioapplications. *Angew. Chem., Int. Ed.* **2021**, *60*, 7476–7487.
- (4) Lin, T. A.; Chatterjee, T.; Tsai, W. L.; Lee, W. K.; Wu, M. J.; Jiao, M.; Pan, K. C.; Yi, C. L.; Chung, C. L.; Wong, K. T.; Wu, C. C. Sky-Blue Organic Light Emitting Diode with 37% External Quantum Efficiency Using Thermally Activated Delayed Fluorescence from Spiroacridine-Triazine Hybrid. *Adv. Mater.* **2016**, *28*, 6976–6983.
- (5) Zhang, D.; Duan, L.; Zhang, Y.; Cai, M.; Zhang, D.; Qiu, Y. Highly Efficient Hybrid Warm White Organic Light-Emitting Diodes Using a Blue Thermally Activated Delayed Fluorescence Emitter: Exploiting the External Heavy-Atom Effect. *Light: Sci. Appl.* **2015**, *4*, No. e232.
- (6) Yamaguchi, Y.; Matsubara, Y.; Ochi, T.; Wakamiya, T.; Yoshida, Z. How the Conjugation Length Affects the Fluorescence Emission Efficiency. *J. Am. Chem. Soc.* **2008**, *130*, 13867–13869.
- (7) An, B. K.; Gierschner, J.; Park, S. Y. Conjugated Cyanostilbene Derivatives: A Unique Self-Assembly Motif for Molecular Nanostructures with Enhanced Emission and Transport. *Acc. Chem. Res.* **2012**, *45*, 544–554.
- (8) Liu, S.; Zhang, H.; Li, Y.; Liu, J.; Du, L.; Chen, M.; Kwok, R. T. K.; Lam, J. W. Y.; Phillips, D. L.; Tang, B. Z. Strategies to Enhance the Photosensitization: Polymerization and the Donor-Acceptor Even-Odd Effect. *Angew. Chem., Int. Ed.* **2018**, *57*, 15189–15193.
- (9) Zhao, J.; Wu, W.; Sun, J.; Guo, S. Triplet Photosensitizers: From Molecular Design to Applications. *Chem. Soc. Rev.* **2013**, *42*, 5323–5351.
- (10) Shen, H.; Li, Y.; Li, Y. Self-Assembly and Tunable Optical Properties of Intramolecular Charge Transfer Molecules. *Aggregate* **2020**, *1*, 57–68.
- (11) Xu, Z.; Wang, C.; Qiao, Q.; Chi, W.; Chen, J.; Liu, W.; Tan, D.; McKechnie, S.; Lyu, D.; Jiang, X.-F.; Zhou, W.; Xu, N.; Zhang, Q.; Liu, X. Quantitative Design of Bright Fluorophores and AIEgens via the Accurate Prediction of Twisted Intramolecular Charge Transfer (TICT). *Angew. Chem., Int. Ed.* **2020**, *59*, 10160–10172.
- (12) Watson, W. F.; Livingston, R. Concentration Quenching of Fluorescence in Chlorophyll Solutions. *Nature* **1948**, *162*, 452–453.
- (13) Tu, Y.; Zhao, Z.; Lam, J. W. Y.; Tang, B. Z. Aggregate Science: Much to Explore in the Meso World. *Matter* **2021**, *4*, 338–349.
- (14) Zhang, H.; Zhao, Z.; Turley, A. T.; Wang, L.; McGonigal, P. R.; Tu, Y.; Li, Y.; Wang, Z.; Kwok, R. T. K.; Lam, J. W. Y.; Tang, B. Z. Aggregate Science: From Structures to Properties. *Adv. Mater.* **2020**, *32*, 2001457.
- (15) Yang, J.; Fang, M.; Li, Z. Organic Luminescent Materials: The Concentration on Aggregates from Aggregation-Induced Emission. *Aggregate* **2020**, *1*, 6–18.
- (16) Luo, J.; Xie, Z.; Lam, J. W.; Cheng, L.; Chen, H.; Qiu, C.; Kwok, H. S.; Zhan, X.; Liu, Y.; Zhu, D.; Tang, B. Z. Aggregation-Induced Emission of 1-Methyl-1,2,3,4,5-Pentaphenylsilole. *Chem. Commun.* **2001**, 1740–1741.
- (17) Zhao, Z.; Zhang, H.; Lam, J. W. Y.; Tang, B. Z. Aggregation-Induced Emission: New Vistas at Aggregate Level. *Angew. Chem., Int. Ed.* **2020**, *59*, 9888–9907.
- (18) Mei, J.; Leung, N. L.; Kwok, R. T.; Lam, J. W.; Tang, B. Z. Aggregation-Induced Emission: Together We Shine, United We Soar! *Chem. Rev.* **2015**, *115*, 11718–11940.
- (19) Yanari, S. S.; Bovey, F. A.; Lumry, R. Fluorescence of Styrene Homopolymers and Copolymers. *Nature* **1963**, *200*, 242–244.
- (20) Ye, R.; Liu, Y.; Zhang, H.; Su, H.; Zhang, Y.; Xu, L.; Hu, R.; Kwok, R. T. K.; Wong, K. S.; Lam, J. W. Y.; Goddard, W. A.; Tang, B. Z. Non-Conventional Fluorescent Biogenic and Synthetic Polymers without Aromatic Rings. *Polym. Chem.* **2017**, *8*, 1722–1727.
- (21) He, B.; Zhang, J.; Zhang, J.; Zhang, H.; Wu, X.; Chen, X.; Kei, K. H. S.; Qin, A.; Sung, H. H. Y.; Lam, J. W. Y.; Tang, B. Z. Clusteroluminescence from Cluster Excitons in Small Heterocyclics Free of Aromatic Rings. *Adv. Sci.* **2021**, *8*, 2004299.
- (22) Pucci, A.; Rausa, R.; Ciardelli, F. Aggregation-Induced Luminescence of Polyisobutene Succinic Anhydrides and Imides. *Macromol. Chem. Phys.* **2008**, *209*, 900–906.
- (23) Yan, J.; Zheng, B.; Pan, D.; Yang, R.; Xu, Y.; Wang, L.; Yang, M. Unexpected Fluorescence from Polymers Containing Dithio/Amino-Succinimides. *Polym. Chem.* **2015**, *6*, 6133–6139.
- (24) Braendle, A.; Perevedentsev, A.; Cheetham, N. J.; Stavrinou, P. N.; Schachner, J. A.; Mösch-Zanetti, N. C.; Niederberger, M.; Caseri, W. R. Homoconjugation in Poly(phenylene methylene)s: A Case Study of Non-:–Conjugated Polymers with Unexpected Fluorescent Properties. *J. Polym. Sci., Part B: Polym. Phys.* **2017**, *55*, 707–720.
- (25) Zhou, Q.; Yang, T.; Zhong, Z.; Kausar, F.; Wang, Z.; Zhang, Y.; Yuan, W. Z. Clustering-Triggered Emission Strategy Towards Tunable Multi-Color Persistent Phosphorescence. *Chem. Sci.* **2020**, *11*, 2926–2933.
- (26) Zhang, H.; Zhao, Z.; McGonigal, P. R.; Ye, R.; Liu, S.; Lam, J. W. Y.; Kwok, R. T. K.; Yuan, W. Z.; Xie, J.; Rogach, A. L.; Tang, B. Z. Clusterization-Triggered Emission: Uncommon Luminescence from Common Materials. *Mater. Today* **2020**, *32*, 275–292.

(27) Wang, Z.; Zhang, H.; Li, S.; Lei, D.; Tang, B. Z.; Ye, R. Recent Advances in Clusteroluminescence. *Top. Curr. Chem.* **2021**, *379*, 14.

(28) Zhang, X.; Du, L.; Zhao, W.; Zhao, Z.; Xiong, Y.; He, X.; Gao, P. F.; Alam, P.; Wang, C.; Li, Z.; Leng, J.; Liu, J.; Zhou, C.; Lam, J. W. Y.; Phillips, D. L.; Zhang, G.; Tang, B. Z. Ultralong UV/Mechano-Excited Room Temperature Phosphorescence from Purely Organic Cluster Excitons. *Nat. Commun.* **2019**, *10*, 5161.

(29) Zhao, Z.; Wang, Z.; Tavakoli, J.; Shan, G.; Zhang, J.; Peng, C.; Xiong, Y.; Zhang, X.; Cheung, T. S.; Tang, Y.; Huang, B.; Yu, Z.; Lam, J. W. Y.; Tang, B. Z. Revisiting an Ancient Inorganic Aggregation-Induced Emission System: An Enlightenment to Clusteroluminescence. *Aggregate* **2021**, *2*, No. e36.

(30) Shao, S.; Wang, L. Through-Space Charge Transfer Polymers for Solution-Processed Organic Light-Emitting Diodes. *Aggregate* **2020**, *1*, 45–56.

(31) Zhang, H.; Zheng, X.; Xie, N.; He, Z.; Liu, J.; Leung, N. L. C.; Niu, Y.; Huang, X.; Wong, K. S.; Kwok, R. T. K.; Sung, H. H. Y.; Williams, I. D.; Qin, A.; Lam, J. W. Y.; Tang, B. Z. Why Do Simple Molecules with “Isolated” Phenyl Rings Emit Visible Light? *J. Am. Chem. Soc.* **2017**, *139*, 16264–16272.

(32) Zhang, J.; Zhang, H.; Lam, J. W. Y.; Tang, B. Z. Restriction of Intramolecular Motion (RIM): Investigating Aie Mechanism from Experimental and Theoretical Studies. *Chem. Res. Chin. Univ.* **2021**, *37*, 1–15.

(33) Tu, Y.; Yu, Y.; Xiao, D.; Liu, J.; Zhao, Z.; Liu, Z.; Lam, J. W. Y.; Tang, B. Z. An Intelligent Aiegen with Nonmonotonic Multiresponses to Multistimuli. *Adv. Sci.* **2020**, *7*, 2001845.

(34) Mu, Y.; Liu, Y.; Tian, H.; Ou, D.; Gong, L.; Zhao, J.; Zhang, Y.; Huo, Y.; Yang, Z.; Chi, Z. Sensitive and Repeatable Photoinduced Luminescent Radicals from a Simple Organic Crystal. *Angew. Chem., Int. Ed.* **2021**, *60*, 6367–6371.

(35) Ai, X.; Evans, E. W.; Dong, S.; Gillett, A. J.; Guo, H.; Chen, Y.; Hele, T. J. H.; Friend, R. H.; Li, F. Efficient Radical-Based Light-Emitting Diodes with Doublet Emission. *Nature* **2018**, *563*, 536–540.

(36) Andersen, P.; Klewe, B. The Crystal Structure of the Free Radical Tri-*p*-nitrophenylmethyl. *Acta Chem. Scand.* **1967**, *21*, 2599–2607.

(37) Zhao, W.; He, Z.; Peng, Q.; Lam, J. W. Y.; Ma, H.; Qiu, Z.; Chen, Y.; Zhao, Z.; Shuai, Z.; Dong, Y.; Tang, B. Z. Highly Sensitive Switching of Solid-State Luminescence by Controlling Intersystem Crossing. *Nat. Commun.* **2018**, *9*, 3044.

(38) Spackman, M. A.; Jayatilaka, D. Hirshfeld Surface Analysis. *CrystEngComm* **2009**, *11*, 19–32.

(39) Leung, N. L.; Xie, N.; Yuan, W.; Liu, Y.; Wu, Q.; Peng, Q.; Miao, Q.; Lam, J. W.; Tang, B. Z. Restriction of Intramolecular Motions: The General Mechanism Behind Aggregation-Induced Emission. *Chem. - Eur. J.* **2014**, *20*, 15349–15353.

(40) Zhang, H.; Liu, J.; Du, L.; Ma, C.; Leung, N. L. C.; Niu, Y.; Qin, A.; Sun, J.; Peng, Q.; Sung, H. H. Y.; Williams, I. D.; Kwok, R. T. K.; Lam, J. W. Y.; Wong, K. S.; Phillips, D. L.; Tang, B. Z. Drawing a Clear Mechanistic Picture for the Aggregation-Induced Emission Process. *Mater. Chem. Front.* **2019**, *3*, 1143–1150.

(41) Shuai, Z.; Peng, Q. Organic Light-Emitting Diodes: Theoretical Understanding of Highly Efficient Materials and Development of Computational Methodology. *Natl. Sci. Rev.* **2017**, *4*, 224–239.

(42) Tu, Y.; Liu, J.; Zhang, H.; Peng, Q.; Lam, J. W. Y.; Tang, B. Z. Restriction of Access to the Dark State: A New Mechanistic Model for Heteroatom-Containing Aie Systems. *Angew. Chem., Int. Ed.* **2019**, *58*, 14911–14914.